New Journal of Physics
The open access journal at the forefront of physics

Deutsche Physikalische Gesellschaft DPG
IOP Institute of Physics

Published in partnership with: Deutsche Physikalische Gesellschaft and the Institute of Physics

OPEN ACCESS

RECEIVED
23 August 2020

REVISED
2 December 2020

ACCEPTED FOR PUBLICATION
4 January 2021

PUBLISHED
20 January 2021

PAPER

Effects of higher levels of qubits on control of qubit protected by a Josephson quantum filter

Shumpei Masuda[1,2,*] and **Kazuki Koshino**[1]

[1] College of Liberal Arts and Sciences, Tokyo Medical and Dental University, Ichikawa, 272-0827, Japan
[2] Research Center for Emerging Computing Technologies, National Institute of Advanced Industrial Science and Technology (AIST), 1-1-1, Umezono, Tsukuba, Ibaraki 305-8568, Japan
[*] Author to whom any correspondence should be addressed.

E-mail: shumpei.masuda@aist.go.jp

Keywords: Josephson quantum filter, transmon, anharmonicity parameter

Abstract

A Josephson quantum filter (JQF) protects a data qubit (DQ) from the radiative decay into transmission lines (TLs) in superconducting quantum computing architectures. A transmon, which is a weakly nonlinear harmonic oscillator rather than a pure two-level system, can play a role of a JQF or a DQ. However, in the previous study, a JQF and a DQ were modeled as two-level systems neglecting the effects of higher levels. We theoretically examine the effects of the higher levels of the JQF and the DQ on the control of the DQ. It is shown that the higher levels of the DQ cause the shift of the resonance frequency and the decrease of the maximum population of the first excited state of the DQ in the controls with a continuous wave (cw) field and a pulsed field, while the higher levels of the JQF do not. Moreover, we present optimal parameters of the pulsed field, which maximize the control efficiency.

1. Introduction

In waveguide quantum electrodynamics (QED) systems, an atom is coupled strongly to a one-dimensional (1D) optical field typically provided by a waveguide or a transmission line (TL), so that spontaneous emission from an atom is mostly forwarded to this one-dimensional field. Such systems are indispensable for realization of distributed quantum computation, in which photonic qubits quantum-mechanically connect distant matter qubits. In contrast with the natural atom–atom interaction, which becomes weaker rapidly as their mutual distance increases, the atom–atom interaction in waveguide QED systems is long-ranged owing to the one-dimensionality of the field.

A waveguide QED system was first realized with a cavity QED system (atom-cavity coupled system) in the bad-cavity regime exploiting the Purcell effect [1]. Waveguide QED systems can be realized also in superconducting circuits, which is a promising platform for quantum information processings [2–11], by coupling a superconducting artificial atom directly to a microwave TL [8, 12, 13]. This enabled us to implement a waveguide QED setup involving several atoms coupled to a common waveguide [14]. In such setups, distant atoms can interact with each other via virtual photons propagating in the waveguide. The coupling between a superconducting artificial atom with a 1D waveguide has been achieved even in the ultrastrong coupling regime [15]. Quantum computation schemes [16, 17], two-photon nonlinearlities and photon correlation function [18] were studied in waveguide QED systems.

Gate operations of qubits should be performed in the coherence times of the qubits for quantum computation. A strong drive field can realize short-time gate operations of a target qubit. However, it can induce unwanted crosstalk of the qubit with neighboring qubits and resonators. A strong coupling between a qubit and its control line can make the gate speed fast even with a weak drive field, but makes the qubit lifetime, T_1, short due to radiative decay through the line. (For the dephasing time T_2^* cannot exceed twice T_1, T_1 ultimately limits the qubit coherence [19].) Therefore, it is important to decrease the radiative decay of a qubit while keeping the coupling between the qubit and the control line sufficiently strong.

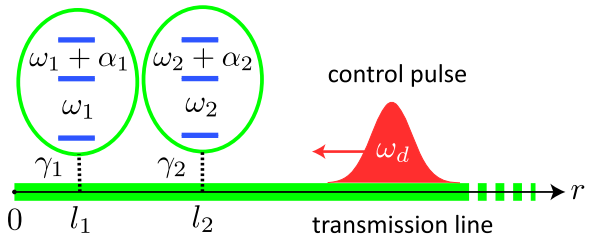

Figure 1. Schematic of the setup. The DQ and the JQF are coupled to a semi-infinite TL, through which control pulses for the DQ is applied.

Various methods to decrease or design qubit decay in circuit QED systems have been studied using, e.g. effect of boundary condition [20], mirror [21], other multiple qubits [14, 22–24] including superconducting metamaterials [25].

It was shown that a qubit attached to a TL with suitable parameters can work as a filter, which prohibits a data qubit (DQ) from radiative decay to the TL [26, 27]. The protecting qubit is called a Josephson quantum filter (JQF). A transmon can work as a JQF or a DQ in superconducting quantum computing architectures. A transmon is a weakly nonlinear harmonic oscillator rather than a pure two-level system [28]. However, in the previous study [26], both the DQ and the JQF were modeled as pure two-level systems neglecting higher levels.

In this paper, we consider controls of the DQ with a continuous wave (cw) field and a pulsed field, which are routinely performed for calibrations of experimental apparatuses, parameter determinations, and quantum information processing. We examine the effects of the higher levels of the qubits and show the shift of the resonance frequency and the change in the maximum fidelity of the controls induced by them. Furthermore, we show optimal parameters for controls with a pulsed field.

The rest of this paper is organized as follows. In section 2, we introduce a model for the system. In section 3, we derive formulae of the resonance frequency and the maximum population of the first excited state of the DQ under a cw field. We numerically study the controls of the DQ with a cw field and a pulsed field in section 4. The results are compared with the theoretical prediction. We present an optimal pulse length for the control with a pulsed field. Section 5 provides a summary.

2. Model

Our system is composed of two qubits, the DQ (qubit 1) and the JQF (qubit 2), attached to a semi-infinite TL, which extends in the $r > 0$ region. The schematic of the setup is illustrated in figure 1. The position, angular frequency, anharmonicity parameter and coupling strength to the TL of qubit $m(= 1, 2)$ are denoted by l_m, ω_m, α_m and γ_m, respectively. When $l_1 < l_2$ and $\gamma_1 \ll \gamma_2$, qubit 2 can work as a JQF, which prohibits the radiative decay of qubit 1 [26]. In this study, we assume that the resonance frequencies of the qubits are identical and that the positions of the qubits are optimal, that is, $l_1 = 0$ and $l_2/\lambda_q = 0.5$, where λ_q is the resonance wavelength of the qubits.

Adopting the units in which $\hbar = v = 1$, where v is the microwave velocity in the TL, the Hamiltonian of the system is represented as

$$H = \sum_m \left(\omega_m c_m^\dagger c_m + \frac{\alpha_m}{2} c_m^\dagger c_m^\dagger c_m c_m\right) + \int_0^\infty \mathrm{d}k \left[k b_k^\dagger b_k + \sum_m g_{mk}(c_m^\dagger b_k + b_k^\dagger c_m)\right], \quad (1)$$

where c_m is the bosonic annihilation operator of qubit m, and $b_{k(>0)}$ is the annihilation operator of the eigenmode of the TL with the wave number k and the mode function, $f_k = \sqrt{2/\pi}\cos kr$, normalized as $\int_0^\infty \mathrm{d}r f_{k'}(r) f_k(r) = \delta(k - k')$. The coupling constant between qubit m and the TL is given by

$$g_{mk} = \sqrt{\frac{\gamma_m}{2}} f_k(l_m) = \sqrt{\frac{\gamma_m}{\pi}}\cos(kl_m), \quad (2)$$

where γ_m represents the radiative decay rate of the first excited state of qubit m, when coupled to an *open* waveguide. By naively applying the Fermi's golden rule, the radiative decay rate of the nth excited level of qubit m to the $(n-1)$th level amounts to $2\pi n|g_{m\omega_m}|^2 = 2n\gamma_m \cos^2(\omega_m l_m)$.

2.1. Equation of motion

The Heisenberg equation for b_k leads to

$$\frac{\mathrm{d}}{\mathrm{d}t}b_k = -ikb_k - i\sum_m g_{mk}c_m, \tag{3}$$

which is formally solved as

$$b_k(t) = b_k(0)\mathrm{e}^{-\mathrm{i}kt} - \mathrm{i}\sum_m g_{mk}\int_0^t \mathrm{d}t' c_m(t')\mathrm{e}^{\mathrm{i}k(t'-t)}. \tag{4}$$

We formally extend the lower limit of k to $-\infty$ in order to introduce the real-space representation of the field operator defined by

$$\tilde{b}_r = \frac{1}{\sqrt{2\pi}}\int_{-\infty}^{\infty}\mathrm{d}k\ \mathrm{e}^{\mathrm{i}kr}b_k. \tag{5}$$

Here, r runs over $-\infty < r < \infty$. The negative and positive regions represent the incoming and outgoing fields, respectively. The introduction of the real-space representation has been validated in reference [29]. Using equations (4) and (5), we obtain

$$\begin{aligned}\tilde{b}_r(t) = \tilde{b}_{r-t}(0) - i\sum_m\sqrt{\frac{\gamma_m}{2}}\left[\Theta_{r\in(-l_m,t-l_m)}c_m(t-r-l_m)\right.\\ \left.+\Theta_{r\in(l_m,t+l_m)}c_m(t-r+l_m)\right],\end{aligned} \tag{6}$$

where $\Theta_{r\in(a,b)} = \theta(r-a)\theta(b-r)$. Using equation (6), we can obtain

$$\begin{aligned}\tilde{b}_{l_m}(t) + \tilde{b}_{-l_m}(t) = \tilde{b}_{l_m-t}(0) + \tilde{b}_{-l_m-t}(0) - i\sum_n\sqrt{\frac{\gamma_n}{2}}\left[c_n(t-l_m-l_n)\right.\\ \left.+c_n(t-|l_m-l_n|)\right].\end{aligned} \tag{7}$$

On the other hand, the Heisenberg equation for a system operator O (composed of qubit operators) is written as

$$\begin{aligned}\frac{\mathrm{d}}{\mathrm{d}t}O = i[H_\mathrm{s},O] + i\sum_m\sqrt{\frac{\gamma_m}{2}}\left([c_m^\dagger,O]\left\{\tilde{b}_{l_m}(t)+\tilde{b}_{-l_m}(t)\right\}\right.\\ \left.+\left\{\tilde{b}_{l_m}^\dagger(t)+\tilde{b}_{-l_m}^\dagger(t)\right\}[c_m,O]\right),\end{aligned} \tag{8}$$

where $H_\mathrm{s} = \sum_m(\omega_m c_m^\dagger c_m + \frac{\alpha_m}{2}c_m^\dagger c_m^\dagger c_m c_m)$ and $[A,B] = AB - BA$. Substitution of equation (7) into equation (8) leads to

$$\begin{aligned}\frac{\mathrm{d}}{\mathrm{d}t}O = i[H_\mathrm{s},O] + i\sum_m\left\{[c_m^\dagger,O]N_m(t) + N_m^\dagger(t)[c_m,O]\right\}\\ +\sum_{m,n}\frac{\sqrt{\gamma_m\gamma_n}}{2}[c_m^\dagger,O]\left\{c_n(t-l_m-l_n)+c_n(t-|l_m-l_n|)\right\}\\ -\sum_{m,n}\frac{\sqrt{\gamma_m\gamma_n}}{2}\left\{c_n^\dagger(t-l_m-l_n)+c_n^\dagger(t-|l_m-l_n|)\right\}[c_m,O],\end{aligned} \tag{9}$$

where $N_m(t)$ is the noise operator defined by

$$N_m(t) = \sqrt{\frac{\gamma_m}{2}}\left[\tilde{b}_{l_m-t}(0)+\tilde{b}_{-l_m-t}(0)\right]. \tag{10}$$

By replacing $c_m(t-\Delta t)$ with $\mathrm{e}^{\mathrm{i}\omega_m\Delta t}c_m$ (free evolution approximation [26]), the equation of motion is rewritten as

$$\begin{aligned}\frac{\mathrm{d}}{\mathrm{d}t}O = i[H_\mathrm{s},O] + i\sum_m\left\{[c_m^\dagger,O]N_m(t) + N_m^\dagger(t)[c_m,O]\right\}\\ +\sum_{m,n}\left(\xi_{mn}[c_m^\dagger,O]c_n - \xi_{mn}^*c_n^\dagger[c_m,O]\right),\end{aligned} \tag{11}$$

where

$$\xi_{mn} = \frac{\sqrt{\gamma_m \gamma_n}}{2}\left(e^{i\omega_q(l_m+l_n)} + e^{i\omega_q|l_m-l_n|}\right). \tag{12}$$

Note that $\omega_1 = \omega_2$ is assumed here, and they are denoted by ω_q.

2.2. Radiative decay

Here, we show how the radiative decay of the DQ is suppressed following the manner used in reference [26]. We assume that only the DQ is excited at the initial moment and no drive field is applied. Then, there is only a single excitation in the whole system during the dynamics because the Hamiltonian conserves the total excitation number. Therefore, higher levels of the DQ and the JQF can be neglected.

Using equation (11), the equation of motion for $c_m (m = 1, 2)$ is written as

$$\frac{d}{dt}c_m = (-i\omega_m - \xi_{mm})c_m - \xi_{mn}c_n - iN_m(t), \tag{13}$$

where $n = 3 - m$. In equation (13), we have omitted terms with α_m because higher levels do not play any roles. The initial state is represented as

$$|\Psi(0)\rangle = c_1^\dagger |v\rangle, \tag{14}$$

where $|v\rangle$ represents the vacuum state of the whole setup. The state at time t can be written as

$$|\Psi(t)\rangle = \sum_{m=1,2} \phi_m(t) c_m^\dagger |v\rangle + \int dr f(r,t)\tilde{b}_r^\dagger |v\rangle, \tag{15}$$

where the coefficient ϕ_m and the wave form of the emitted photon $f(r, t)$ satisfy the normalization condition, $\sum_m |\phi_m(t)|^2 + \int_0^t dr |f(r,t)|^2 = 1$. Coefficient ϕ_m can be written as

$$\phi_m(t) = \langle v|c_m|\Psi(t)\rangle = \langle v|c_m(t)c_1^\dagger(0)|v\rangle \tag{16}$$

using the fact that $H|v\rangle = 0$.

Using equations (13) and (16), we obtain the equations of motion for ϕ_m as

$$\begin{aligned}\frac{d}{dt}\phi_1 &= -(i\omega_q + \xi_{11})\phi_1 - \xi_{12}\phi_2,\\ \frac{d}{dt}\phi_2 &= -\xi_{21}\phi_1 - (i\omega_q + \xi_{22})\phi_2.\end{aligned} \tag{17}$$

The initial conditions are $\phi_1(0) = 1$ and $\phi_2(0) = 0$. A solution of equation (17) is represented as

$$\begin{aligned}\phi_1(t) &= \left(\frac{\mu_2 + \xi_{11}}{\mu_2 - \mu_1} e^{\mu_1 t} + \frac{\mu_1 + \xi_{11}}{\mu_1 - \mu_2} e^{\mu_2 t}\right) e^{-i\omega_q t},\\ \phi_2(t) &= \frac{\xi_{21}}{\mu_2 - \mu_1}(e^{\mu_1 t} - e^{\mu_2 t})e^{-i\omega_q t},\end{aligned} \tag{18}$$

where μ_1 and μ_2 are the solutions of a quadratic equation for z, $(z + \xi_{11})(z + \xi_{22}) - \xi_{12}\xi_{21} = 0$.

With an optimal choice of $l_{1,2}$, $l_1 = 0$ and $l_2/\lambda_q = 0.5$, we have $\xi_{11} = \gamma_1$, $\xi_{22} = \gamma_2$, and $\xi_{12} = \xi_{21} = -\sqrt{\gamma_1\gamma_2}$. Then, equation (18) is rewritten as

$$\begin{aligned}\phi_1(t) &= \left(\frac{\gamma_2}{\gamma_1 + \gamma_2} + \frac{\gamma_1}{\gamma_2 + \gamma_2} e^{-(\gamma_1+\gamma_2)t}\right) e^{-i\omega_q t},\\ \phi_2(t) &= \frac{\sqrt{\gamma_1\gamma_2}}{\gamma_1 + \gamma_2}[1 - e^{-(\gamma_1+\gamma_2)t}]\, e^{-i\omega_q t}.\end{aligned} \tag{19}$$

Thus, the survival probability of the DQ is approximately unity, i.e. $|\phi_1(t)|^2 \approx 1$, when $\gamma_2 \gg \gamma_1$. This stabilization of the DQ is due to the photon-mediated interaction between the DQ and JQF. (We refer to reference [26] for more details.)

2.3. Dynamics under control field

We assume that the qubits are in the ground state at the initial time, and that a classical control field $E_{in}(t)$ is applied for $t > 0$. The spatial waveform of the control field at $t = 0$ is represented as $E_{in}(-r)$. The initial state vector is written as

$$|\phi(0)\rangle = N \exp\left(\int_{-\infty}^{0} dr\, E_{in}(-r)\tilde{b}_r^\dagger\right)|v\rangle, \tag{20}$$

where $N = \exp(-\int \mathrm{d}r|E_{\mathrm{in}}(-r)|^2/2)$ is a normalization factor, and $|v\rangle$ is the overall ground state, the product state of the ground states of two qubits and the vacuum states of the waveguide modes. The control field is represented as

$$E_{\mathrm{in}}(t) = 2E_{\mathrm{d}}(t)\ \cos(\omega_{\mathrm{d}}t) \tag{21}$$

where the frequency and the envelope of the control field are $\omega_{\mathrm{d}}/2\pi$ and E_{d}, respectively.

We can determine the reduced density matrix of the system (the DQ and the JQF) from equation (11) as follows. By definition, the reduced density matrix of the system at time t is written as

$$\rho_{\mathrm{s}}(t) = \mathrm{Tr}_{\mathrm{TL}}[U(t)|\phi(0)\rangle\langle\phi(0)|U^{\dagger}(t)], \tag{22}$$

where $U(t) = \mathrm{e}^{-\mathrm{i}Ht}$ denotes the time evolution operator of the whole system, and $\mathrm{Tr}_{\mathrm{TL}}$ means taking the partial trace on the photon modes in the TL. We introduce the transition operator of the system defined by

$$S_{m'n'\,mn} = |m'n'\rangle\langle mn|, \tag{23}$$

where the first and second indices in the state vector represent the excitation number of the DQ and the JQF, respectively. In the Heisenberg picture, the expectation value of this operator is given by

$$\langle S_{m'n'mn}(t)\rangle = \langle\phi(0)|S_{m'n'mn}(t)|\phi(0)\rangle. \tag{24}$$

Using $S_{m'n'mn}(t) = U^{\dagger}(t)S_{m'n'mn}(0)U(t)$, the above quantity can be rewritten as

$$\langle S_{m'n'mn}(t)\rangle = \langle mn|\rho_{\mathrm{s}}(t)|m'n'\rangle = \rho_{m,n,m',n'}(t). \tag{25}$$

Thus, the reduced density matrix elements are determined as the expectation values of the transition operators. From equation (25), we have

$$\dot{\rho}_{m,n,m',n'}(t) = \langle\dot{S}_{m'n'mn}(t)\rangle, \tag{26}$$

where the dot denotes the time derivative. The right-hand side of equation (26) can be rewritten in terms of $\rho_{k,l,k',l'}(t)$ by using equation (11) with $O = S_{m'n'mn}$ (see appendix C).

3. Effects of a higher level in cw drive

We consider a cw drive of the DQ protected by the JQF. As shown in the following section, we observe the shift of the resonance frequency and the decrease of maximum population of the first excited state in Rabi oscillations. We attribute these to the second excited state of the DQ, and derive analytic formulae of the resonance frequency and the maximum population with the use of an effective Hamiltonian, which consists of a transmom under a control field.

The effective time-dependent Hamiltonian describing the DQ is given by

$$H(t) = \omega c^{\dagger}c + \frac{\alpha}{2}c^{\dagger}c^{\dagger}cc + 2\Omega\ \cos(\omega_{\mathrm{d}}t)(c^{\dagger} + c), \tag{27}$$

where $\omega = \omega_{\mathrm{q}}$, $\alpha = \alpha_1 < 0$ and $c = c_1$. Here, Ω is the Rabi frequency, which is related to the control field by $\Omega = \sqrt{2\gamma_1}E_{\mathrm{d}}$. As we observe later appendix (A), when $\gamma_{1,2} \ll |E_{\mathrm{d}}|^2$, the dynamics of the DQ is mainly governed by the applied field and the mutual interaction with the JQF is negligible. Therefore, assuming such a strong drive regime, we neglect the existence of JQF in this section.

Now, we consider a subsystem spanned by three levels $|0\rangle$, $|1\rangle$ and $|2\rangle$. The Hamiltonian is represented as

$$H = \begin{pmatrix} 0 & 2\Omega\ \cos(\omega_{\mathrm{d}}t) & 0 \\ 2\Omega\ \cos(\omega_{\mathrm{d}}t) & \omega & 2\sqrt{2}\Omega\ \cos(\omega_{\mathrm{d}}t) \\ 0 & 2\sqrt{2}\Omega\ \cos(\omega_{\mathrm{d}}t) & 2\omega + \alpha \end{pmatrix}. \tag{28}$$

We move to a rotating frame with angular frequency of ω_{d} and use the rotating wave approximation to rewrite the Hamiltonian as

$$H = \begin{pmatrix} 0 & \Omega & 0 \\ \Omega & \omega - \omega_{\mathrm{d}} & \sqrt{2}\Omega \\ 0 & \sqrt{2}\Omega & 2(\omega - \omega_{\mathrm{d}}) + \alpha \end{pmatrix}. \tag{29}$$

We consider a subspace expanded by $|1\rangle$, $|2\rangle$ in which the Hamiltonian is represented as

$$H_2 = \begin{pmatrix} \omega - \omega_{\mathrm{d}} & \sqrt{2}\Omega \\ \sqrt{2}\Omega & 2(\omega - \omega_{\mathrm{d}}) + \alpha \end{pmatrix} = \frac{3(\omega - \omega_{\mathrm{d}}) + \alpha}{2}I_{(2)} + \begin{pmatrix} a & b \\ b & -a \end{pmatrix}, \tag{30}$$

where $I_{(2)}$ is the identity operator and

$$a = \frac{-\alpha - \omega + \omega_{\rm d}}{2},$$
$$b = \sqrt{2}\Omega. \tag{31}$$

The eigenenergies are represented as

$$E_{\pm} = \frac{3(\omega - \omega_{\rm d}) + \alpha}{2} \pm \sqrt{a^2 + b^2}, \tag{32}$$

and the corresponding eigenstates are written as

$$|\pm\rangle = \cos\,\theta_{\pm}|1\rangle + \sin\,\theta_{\pm}|2\rangle, \tag{33}$$

where

$$\tan\,\theta_{\pm} = \frac{-a \pm \sqrt{a^2 + b^2}}{b}. \tag{34}$$

Alternatively, the eigenstates are represented as

$$|\pm\rangle = -\frac{b}{s_{\pm}}|1\rangle + \frac{a \mp \sqrt{a^2 + b^2}}{s_{\pm}}|2\rangle \tag{35}$$

with

$$s_{\pm} = \left\{2\sqrt{a^2 + b^2}(\sqrt{a^2 + b^2} \mp a)\right\}^{1/2}. \tag{36}$$

We rewrite the Hamiltonian in equation (29) with the basis set $\{|0\rangle, |+\rangle, |-\rangle\}$. In the matrix representation, the Hamiltonian is represented as

$$H = \begin{pmatrix} 0 & \Omega\,\cos\,\theta_{+} & \Omega\,\cos\,\theta_{-} \\ \Omega\,\cos\,\theta_{+} & E_{+} & 0 \\ \Omega\,\cos\,\theta_{-} & 0 & E_{-} \end{pmatrix}. \tag{37}$$

Note that $|+\rangle \simeq |1\rangle$ when $\Omega/|\alpha|$ is sufficiently small. We also emphasize that $\cos\theta_{+} \simeq 1 \gg \cos\theta_{-}$. Therefore, $|-\rangle$ can be neglected, and a Rabi oscillation will be observed between $|0\rangle$ and $|+\rangle$ when parameters are chosen so that $E_{+} = 0$. We regard $E_{+} = 0$ as the resonance condition. For example, $\omega_{\rm d}$ can be tuned to satisfy the resonance condition. The deviation of $\omega_{\rm d}$ from ω is the origin of the shift of the resonance frequency.

Now we derive an analytic form of the shift of the resonance frequency. When $\Omega/|\alpha| \ll 1$, we have $a \gg b$. Then, we obtain from equation (32)

$$E_{+} \simeq \omega - \omega_{\rm d} + \frac{2\Omega^2}{-\alpha - \omega + \omega_{\rm d}}, \tag{38}$$

where we used $\sqrt{a^2 + b^2} \simeq a + b^2/2a$. Thus, we obtain

$$\omega_{\rm d} \simeq \omega + \frac{2\Omega^2}{-\alpha - \omega + \omega_{\rm d}}, \tag{39}$$

when $E_{+} = 0$. Assuming $\omega_{\rm d} \simeq \omega$, we can derive a simple resonance condition

$$\omega_{\rm d} - \omega \simeq -\frac{2\Omega^2}{\alpha}. \tag{40}$$

This represents the shift of the resonance frequency as a function of Ω and α. This shift of the resonance frequency can be understood as follows. When $\alpha < 0 (> 0)$, level $|2\rangle$ is below (above) level $|1\rangle$ in the rotating frame at $\omega_{\rm d}$, assuming a small detuning, $|\omega - \omega_{\rm d}| < |\alpha|$. The interaction between $|1\rangle$ and $|2\rangle$ induced by the drive field pushes upward (downward) level $|1\rangle$. Thus, the resonance frequency is increased (decreased). The shift becomes larger for smaller $|\alpha|$ and larger Ω.

Equation (35) shows that the maximum population of $|1\rangle$ during the Rabi oscillation between $|0\rangle$ and $|+\rangle$ is given by

$$p_{1,\rm cw}^{\rm max} = \frac{b^2}{s^2}. \tag{41}$$

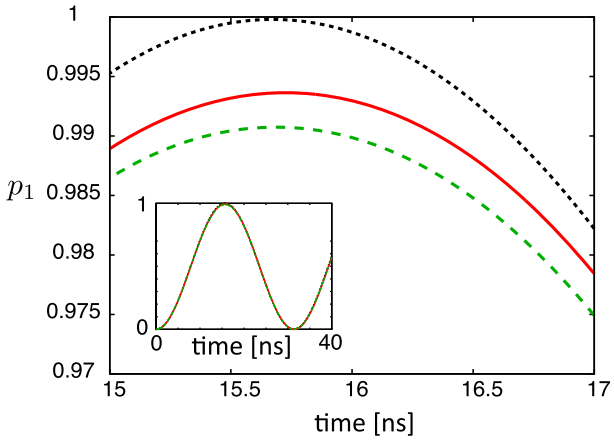

Figure 2. Time dependence of the population of the first excited state of the DQ, p_1, under the cw control field. The used parameter set is $\alpha/2\pi = -300$ MHz, $\omega_{1,2}/2\pi = 5$ GHz, $\gamma_1/2\pi = 2$ kHz, $\gamma_2/2\pi = 100$ MHz and $\sqrt{2\gamma_1}E_d/2\pi = 16$ MHz. Higher levels are taken into account for the data represented by the red solid and the green dashed curves, while the black dotted curve corresponds to the system where the qubits are modeled as two-level systems. The frequency of the control field is $\omega_d/2\pi = 5$ GHz for the green dashed and the black dotted curves, while $\omega_d/2\pi = 5.0017$ GHz for the red solid curve, which is optimized to give the highest value of p_1. Inset: the same plot for a wider time range. Three lines are mostly overlapping.

By using $\Omega/|\alpha| \ll 1$ and $a \simeq -\alpha/2$, an approximate form of the maximum population can be derived as

$$p_{1,\mathrm{cw}}^{\max} \simeq 1 - \frac{2\Omega^2}{\alpha^2}. \tag{42}$$

The same formula can be obtained using Schrieffer–Wolff transformation (see appendix B). The decrease of $p_{1,\mathrm{cw}}^{\max}$ with respect to the increase of $|\Omega|$ and the decrease of $|\alpha|$ can be understood as follows: the interaction between $|1\rangle$ and $|2\rangle$ makes $|+\rangle$ a composite of them. The portion of $|2\rangle$ increases with the increase of $|\Omega|$ and the decrease of $|\alpha|$. Therefore, $p_{1,\mathrm{cw}}^{\max}$ is decreased with the increase of $|\Omega|$ and the decrease of $|\alpha|$.

4. Numerical results

In this section, we numerically examine controls of the DQ with a cw field and with a Gaussian pulse focusing on the shift of the resonance frequency and the maximum value of the population, p_1, of the first excited state of the DQ. The numerical results are compared with the theoretical prediction in section 3 for the control with a cw field. An optimal pulse length is presented for the control with a Gaussian pulse. It is also shown that the maximum value of p_1 for the control with a Gaussian pulse is higher than the one for the control with a cw field.

4.1. cw drive

We simulate the dynamics of the system under a cw control field and calculate the population of the first excited state of the DQ defined by $p_1 = \langle \Pi_1 \otimes I \rangle$, where Π_1 is the projection operator to the first excited state of the DQ and I denotes the identity operator for the JQF. Figure 2 shows the time dependence of p_1. As a reference, we also calculate the dynamics of the system, where both of the DQ and the JQF are modeled as two-level systems, under the cw field with $\omega_d = \omega_q$ (dotted line in figure 2). The maximum value of p_1 is slightly less than unity due to the effects of the JQF [26]. On the other hand, the maximum value of p_1 for the system in which higher levels are taken into account is further lowered even if the frequency of the control field is optimized (solid line in figure 2). In the optimization, we numerically simulated the dynamics of the system for various values of ω_d and looked for $\omega_d = \omega_d^{\mathrm{res}}/2\pi$, which maximizes the maximum value of p_1.

The optimized frequency of the control field, $\omega_d^{\mathrm{res}}/2\pi$, deviates from the resonance frequency of a bare qubit. Figure 3(a) shows $\omega_d^{\mathrm{res}}/2\pi$ as a function of α. The other parameters used are the same as those in figure 2. It is observed that $\omega_d^{\mathrm{res}}/2\pi$ increases linearly with respect to $-1/\alpha$ and is consistent with the analytic expression in equation (40).

Figure 3(b) shows the maximum value of p_1 denoted by $p_{1,\mathrm{cw}}^{\max}$ as a function of $1/\alpha$. It is seen that $p_{1,\mathrm{cw}}^{\max}$ decreases when the anharmonicity parameter $-\alpha$ decreases because the higher excited states become more populated. The numerical result agrees with the theoretical prediction in equations (41) and (42) although $p_{1,\mathrm{cw}}^{\max}$ is slightly lower than the theoretical result. We attribute the difference between the numerical and the

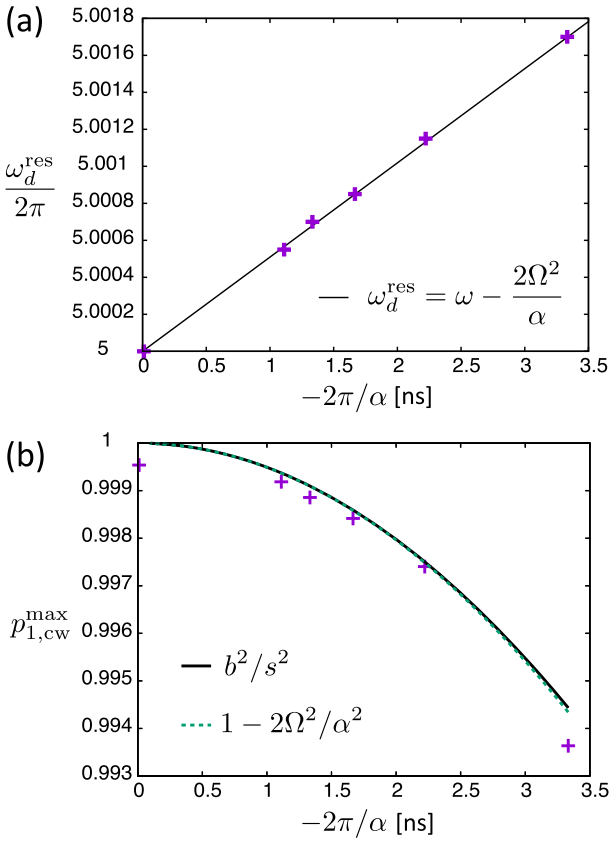

Figure 3. (a) Resonance frequency, $\omega_{\rm d}^{\rm res}/2\pi$, for cw drive for various values of α. The solid line corresponds to the theoretical prediction in equation (40). (b) Maximum value of p_1 for various values of α. The solid and the dotted curves, which are almost overlapping, represent theoretical prediction in equations (41) and (42), respectively. The other parameters used are the same as those in figure 2.

theoretical result to the finite coupling between $|0\rangle$ and $|-\rangle$. The JQF and the levels of the DQ higher than its second excited state also contribute to the difference because the difference becomes smaller when they are omitted.

Similar decrease of the maximum value of p_1 occurs even if the drive amplitude, $E_{\rm d}$, is gradually increased. We consider the case in which $E_{\rm d}$ is increased with a Gaussian form and becomes constant. $E_{\rm d}$ is represented as

$$E_{\rm d}(t) = \begin{cases} E_{\rm amp}\ \exp\left(-4\ \ln\ 2\frac{(t-t_0)^2}{\sigma^2}\right) & \text{for } t < t_0, \\ E_{\rm amp} & \text{for } t \geqslant t_0. \end{cases} \tag{43}$$

The time dependence of $E_{\rm d}$ is shown in figure 4(a). Figure 4(b) shows the time dependences of p_1 under the drive with $E_{\rm d}$ in equation (43) and the drive with

$$E_{\rm d}(t) = E_{\rm amp}\theta(t - t_0'), \tag{44}$$

where θ is the Heaviside step function. Here, t_0' is set so that the pulse areas of the both controls are the same. The maximum values of p_1 in the both controls are approximately 0.994.

4.2. Pulsed drive

We consider a π pulse control aiming at a bit flip of the DQ from the ground state. In this study, we consider a Gaussian pulse represented as

$$E_{\rm d}(t) = E_{\rm amp}\ \exp\left(-4\ \ln\ 2\frac{(t-t_0)^2}{\sigma^2}\right), \tag{45}$$

where t_0, σ, $E_{\rm amp}$ are the pulse center, full width at half maximum and the height of the pulse, respectively. Figure 5 shows the time dependence of p_1 during the control. The frequency and the amplitude of the drive field are optimized for σ of 10 ns to maximize p_1 after the pulse injection. In the optimization, we simulated the dynamics with various values of $\omega_{\rm d}$ and $E_{\rm amp}$ and looked for the values, which maximizes p_1 after the

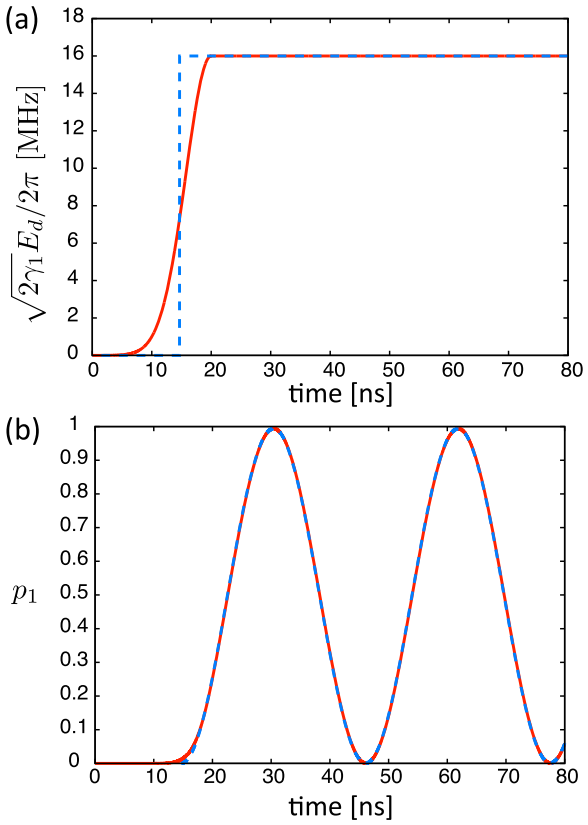

Figure 4. (a) Time profiles of the drive field: equation (43) (red solid curve) and equation (44) (blue dashed curve). (b) Time dependences of p_1 under the drive with E_d in equation (43) (red solid curve) and equation (44) (blue dashed curve). We set $\sqrt{2\gamma_1}E_{\rm amp}/2\pi = 16$ MHz, $\omega_d/2\pi = 5.0017$ GHz, $\sigma = 10$ ns, $t_0 = 20$ ns and $t_0' = 14.7$ ns. The other parameters used are the same as those in figure 2.

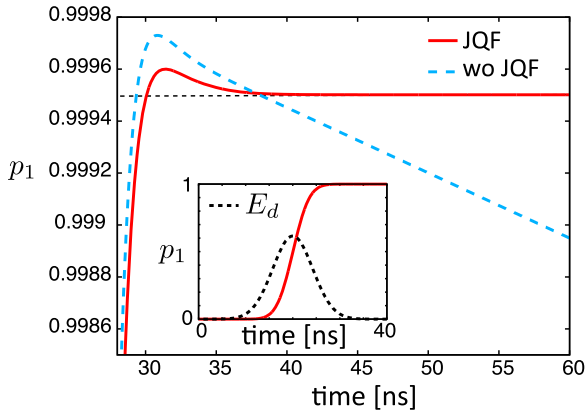

Figure 5. Time dependence of p_1 under the drive with a Gaussian pulse with $\sigma = 10$ ns and $t_0 = 20$ ns. The red solid curve is for the model, which takes into account the higher levels of the DQ. The four lowest levels of DQ and the two lowest levels of the JQF are taken into account. The blue dashed curve is for the system without JQF. The other parameters used are the same as those in figure 2. The horizontal dotted line represents $p_{1,p}^{\rm opt}$. The inset shows p_1 and the pulse envelope in an arbitrary unit for $0 \leqslant t \leqslant 40$ ns.

pulse injection. p_1 is increased up to 0.9995 in spite of the existence of the higher levels, and it becomes stationary after the control because the JQF prohibits unwanted radiative decay of the DQ (solid line in figure 5). This insensitivity of the control efficiency to the higher levels is attributed to the narrow distribution of the pulse field in the frequency space. The full width at half maximum of the pulse field in the frequency space is approximately 88 MHz, and it is smaller than the absolute value of the anharmonicity parameter. The comparison with the result for the system without JQF in which p_1 decreases exponentially with time due to the radiative decay to the TL after the pulse injection, highlights the protection of the DQ by the JQF (dotted line in figure 5).

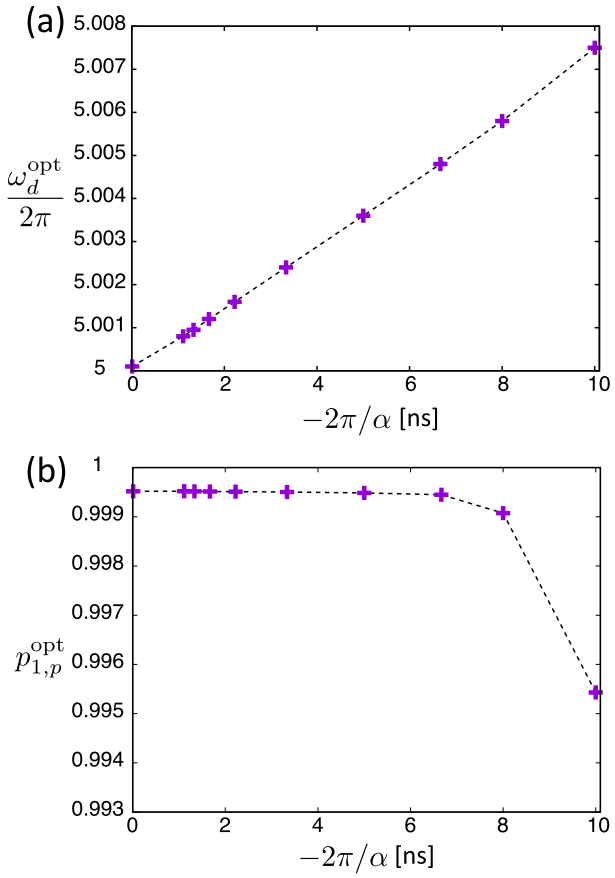

Figure 6. (a) Optimal drive frequency, $\omega_{\rm d}^{\rm opt}/2\pi$, for a pulsed drive with $\sigma = 10$ ns for various values of α. The dotted line is guide to the eye. (b) $p_{1,p}^{\rm opt}$ for various values of α. The other parameters used are the same as those in figure 2.

The optimal drive frequency, $\omega_{\rm d}^{\rm opt}/2\pi$, which maximizes p_1 after the pulse injection, is shown as a function of α in figure 6(a). The frequency and the amplitude of the drive field are optimized for each α. The shift of the optimal drive frequency increases almost linearly with respect to $-1/\alpha$ similar to the case with the cw drive. The maximum value of p_1 after the π pulse control, $p_{1,p}^{\rm opt}$, in figure 6(b) is insensitive to $-1/\alpha$ for $-2\pi/\alpha < 5$ ns and is high compared to the case of the cw drive in figure 3. However, $p_{1,p}^{\rm opt}$ decreases as $-1/\alpha$ increases further because higher levels become more populated when the anharmonicity, $|\alpha|$, of the qubit becomes small.

Figure 7 shows $p_{1,p}^{\rm opt}$ as a function of σ. The frequency and the amplitude of the drive field are optimized for each σ. We have calculated $p_{1,p}^{\rm opt}$ also for the system where the DQ and the JQF are modeled as two-level systems ($|\alpha| \to \infty$), to highlight the decrease of $p_{1,p}^{\rm opt}$ in the case with higher levels. For the system with two-level qubits, $p_{1,p}^{\rm opt}$ decreases monotonically with respect to σ. This is due to the following reason: the JQF does not protect the DQ from radiative decay while the control field is applied due to saturation of the JQF [26]. Thus, the decay of the DQ is enhanced as the control pulse becomes longer. In contrast, there is a peak of $p_{1,p}^{\rm opt}$ at $\sigma = 5$ ns when the higher levels are taken into account. When $\sigma < 5$ ns, $p_{1,p}^{\rm opt}$ drops because the spectral width of the drive pulse becomes large and causes unwanted transitions to the higher levels of the DQ. We have confirmed that $p_{1,p}^{\rm opt}$ is insensitive to the existence of the higher levels of the JQF (see appendix A). For $\sigma > 5$ ns, the behavior of $p_{1,p}^{\rm opt}$ is similar to the case with two-level qubits, although it is slightly lower.

4.3. Comparison between cw and pulsed drives

We compare the controls with a cw field and a Gaussian pulse of which $E_{\rm d}$ is defined in equations (43) and (45), respectively. Figures 8(a) and 8(b) show the time evolution of $E_{\rm d}$ and p_1 during the controls. The maximum p_1 for a Gaussian pulse is higher than the one for a cw field. In the control with a Gaussian pulse, p_1 is sufficiently higher than 0.999, while it increases only up to 0.988 in the control with the cw field. This is because the narrow distribution of Gaussian pulse in the frequency space decreases the effects of the

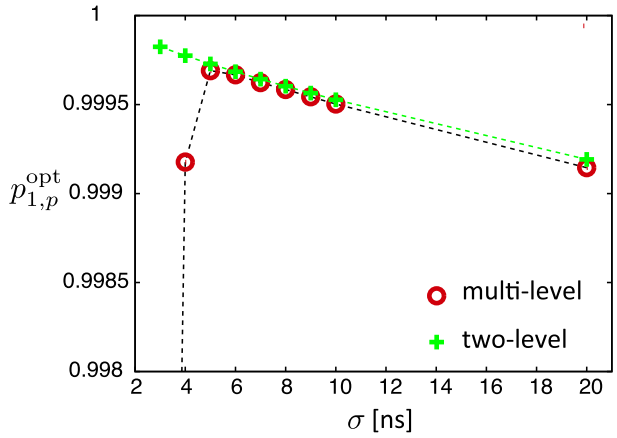

Figure 7. $p_{1,p}^{\rm opt}$ as a function of the pulse length σ. The circles (crosses) are for the system with (without) higher levels. The dashed lines are guide to the eye. The other parameters used are the same as those in figure 2. The four lowest levels of DQ and the two lowest levels of the JQF are taken into account. (see appendix A for the results with more levels of the JQF).

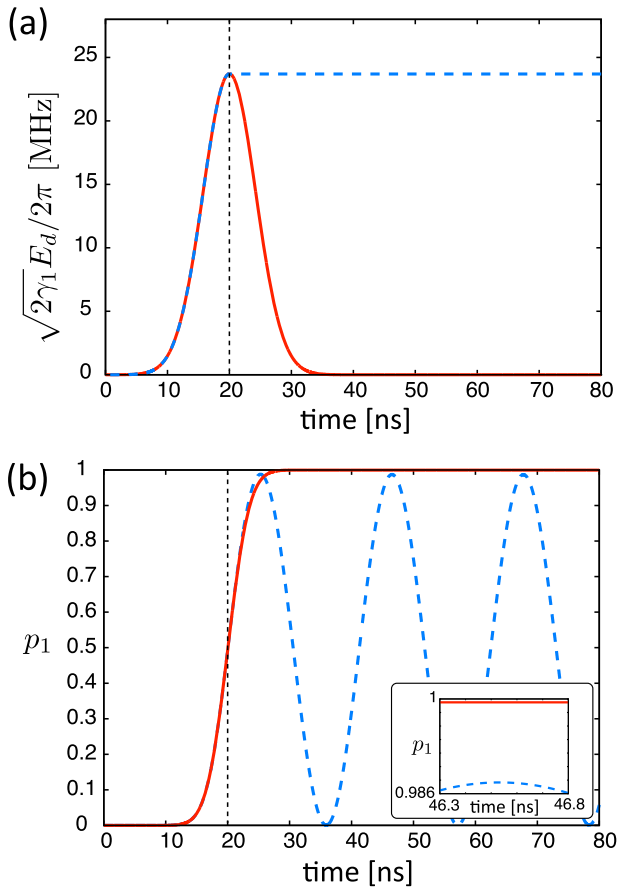

Figure 8. (a) Time dependence of $E_{\rm d}$ in the controls with a cw field (blue dashed curve) and a Gaussian pulse (red solid curve). The vertical lines represent the position of the peak of the Gaussian pulse. (b) Time dependence of p_1 corresponding to $E_{\rm d}$ in panel (a). The inset is a closeup around the second peak of p_1 in the control with a cw field. The used parameter set is $\sigma = 10$ ns and $\sqrt{2\gamma_1}E_{\rm amp}/2\pi = 23.7$ MHz. We used the optimal drive frequencies of 5.0030 GHz and 5.0024 GHz for the controls with a cw field and a Gaussian pulse, respectively. The other parameters used are the same as those in figure 2.

higher levels of the DQ (The width of the pulse in the frequency space is narrower than the anharmonicity parameter), while the population of $|2\rangle$ decreases p_1 in the control with the cw field as shown in section 3.

5. Summary

We have studied the effects of the higher levels of qubits on controls of the DQ protected by a JQF. It has been shown that the higher levels of the DQ cause the shift of the resonance frequency and the decrease of the maximum population of the first excited state in the controls with a cw field and a pulsed field, while the higher levels of the JQF can be neglected. The resonance frequency shift and the time evolution of the populations of the DQ under a cw field has been explained using a simplified model, which leads to simple formulae of the resonance frequency and the population matching well to the numerical results. These results will be useful for the parameter determinations of the system with a cw field.

We have numerically examined the control with a pulsed field aiming at transferring the population to the first excited state of the DQ from the ground state. We have obtained the shift of the resonance frequency, which is inversely proportional to the anharmonicity parameter similarly to the cw drive. In contrast to the cw drive, the maximum population of the first excited state is insensitive to the anharmonicity parameter and is considerably higher the one of the cw drive, when the intensity of the anharmonicity parameter is sufficiently large. The insensitivity of the control efficiency to the higher levels is attributed to the narrow distribution of the pulse field in the frequency space. Moreover, we have shown optimal parameters of the pulsed field, which maximize the control efficiency.

Acknowledgments

We thank T Ishikawa for useful comments. This work was supported in part by the Japan Society for the Promotion of Science (JSPS) Grants-in-Aid for Scientific Research (KAKENHI) (Grants No. 18K03486 and No. 19K03684), the Japan Science and Technology Agency (JST) Exploratory Research for Advanced Technology (ERATO) (Grant No. JPMJER1601), and the Ministry of Education, Culture, Sports, Science, and Technology Quantum Leap Flagship Program (MEXT Q-LEAP) (Grant No. JPMXS0118068682).

Appendix A. Higer levels of JQF

We simulate the dynamics of the system under the drive with a Gaussian pulse, taking into account the higher levels of the JQF. In our numerical simulations, we take into account $N_{\rm JQF}$ lowest levels of the JQF. We numerically solve equation (C.1) moving to a rotating frame at $\omega_{\rm d}$ for the DQ and the JQF with the use of the rotating wave approximation (see appendix C for detail). The Gaussian pulse is the same as the one used in figure 5 for $N_{\rm JQF} = 2$. Figure A1 shows the time dependence of p_1. p_1 for larger $N_{\rm JQF}$ is slightly lower than the one for $N_{\rm JQF} = 2$ due to the disturbance by the higher levels. It is seen that p_1 converges with respect to the increase of $N_{\rm JQF}$.

The dynamics of the DQ shown in figure A1 is insensitive to the higher levels of the JQF. We attribute to this insensitivity to the following. The DQ is driven by two different mechanisms: the mutual interaction with the JQF and the drive field. The intensity of the mutual interaction and the drive field are $|\xi_{12}|$ and $|\langle N_1\rangle|$ in equation (C.2), respectively. In our simulations, we have $|\xi_{12}| \ll |\langle N_1\rangle|$ near the pulse center. In this strong drive regime, the dynamics of the DQ is governed mainly by the drive field. On the other hand, the JQF is lossy much more the DQ. Thus, it approaches rapidly to a mixed state. Figure A2 shows the time dependence of $\langle |i\rangle\langle i| \otimes I_2\rangle$, $\langle I_1 \otimes |i\rangle\langle i|\rangle$, $|\langle |i\rangle\langle i+1| \otimes I_2\rangle|$ and $|\langle I_1 \otimes |i\rangle\langle i+1|\rangle|$, where I_m and $\langle A\rangle$ denote the identity operator of qubit m and the expectation value of A, respectively. Near the pulse center ($|t - t_0| < \sigma/2$), the DQ is changed from the ground state to the first excited state. On the other hand, the rapid change of the JQF is observed in $|t - t_0| > \sigma/2$ when the drive field is relatively weak. The state of the JQF can be approximated by a mixed state near the pulse center.

Appendix B. Analysis with Schrieffer–Wolff transformation

We derive the shift of the resonance frequency and the decrease of maximum population of the first excited state in Rabi oscillations using the Schrieffer–Wolff transformation.

In the rotating frame at $\omega_{\rm d}$, the Hamiltonian is represented as

$$H = H_0 + H_1 + V, \tag{B.1}$$

with

$$H_0 = \varepsilon_1\sigma_{11} + \varepsilon_2\sigma_{22}$$

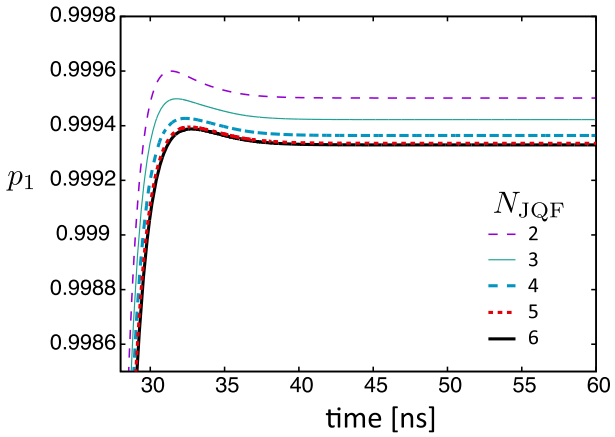

Figure A1. Time dependence of p_1 under the drive with a Gaussian pulse, where N_{JQF} is the number of the levels of the JQF taken into account. The other parameters are the same as those in figure 5.

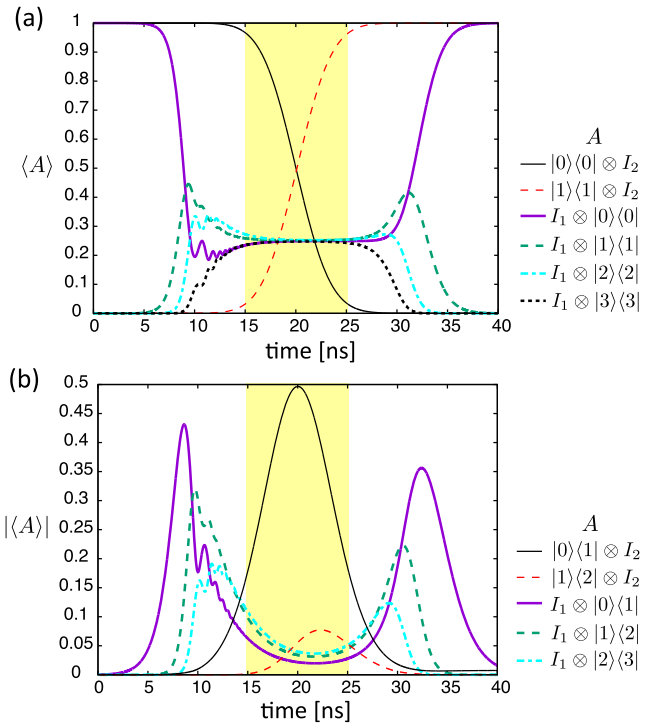

Figure A2. (a) Time dependence of $\langle |i\rangle\langle i| \otimes I_2 \rangle$ and $\langle I_1 \otimes |i\rangle\langle i| \rangle$, (b) time dependence of $|\langle |i\rangle\langle i+1| \otimes I_2 \rangle|$ and $|\langle I_1 \otimes |i\rangle\langle i+1| \rangle|$ for $N_{\mathrm{JQF}} = 4$ and $N_{\mathrm{DQ}} = 4$, where N_{DQ} is the number of the levels of the DQ taken into account. The yellow color represents the time domain: $|t - t_0| < \sigma/2$. The other parameters are the same as those in figure 5.

$$H_1 = \Omega(\sigma_{01} + \sigma_{10})$$
$$V = \sqrt{2}\Omega(\sigma_{12} + \sigma_{21}), \tag{B.2}$$

where we take into account only three levels $|0\rangle$, $|1\rangle$ and $|2\rangle$. Here, $\varepsilon_1 = \omega - \omega_{\mathrm{d}}$, $\varepsilon_2 = 2(\omega - \omega_{\mathrm{d}}) + \alpha$ and $\sigma_{ij} = |i\rangle\langle j|$. We transform the Hamiltonian (Schrieffer–Wolff transformation) as

$$\begin{aligned} H' &= e^{-(S_1+S_2)} H e^{S_1+S_2} \\ &= H_0 + H_1 + V + [H_0, S_1] \\ &\quad + [H_1, S_1] + [V, S_1] + \frac{1}{2}[[H_0, S_1], S_1] + [H_0, S_2] + \cdots . \end{aligned} \tag{B.3}$$

We choose $S_{1,2}$ to diagonalize H' up to $O(\Omega^2)$ except for H_1, which is responsible for Rabi oscillation. Here, S_1 is determined by $V + [H_0, S_1] = 0$ as

$$S_1 = -i\int_{-\infty}^{0} \mathrm{d}t V(t) = \frac{\sqrt{2}\Omega}{\varepsilon_2 - \varepsilon_1}(\sigma_{12} - \sigma_{21}). \tag{B.4}$$

S_2 is determined by $[H_1, S_1] + [V, S_1] + \frac{1}{2}[[H_0, S_1], S_1] + [H_0, S_2] = 0$, which is rewritten as $[H_1, S_1] + [V, S_1]/2 + [H_0, S_2] = 0$. Since $\frac{1}{2}[V, S_1] = \frac{2\Omega^2}{\varepsilon_2 - \varepsilon_1}(\sigma_{22} - \sigma_{11})$ is already diagonal, we choose S_2 to satisfy $[H_1, S_1] + [H_0, S_2] = 0$. Since $[H_1, S_1] = \frac{2\Omega^2}{\varepsilon_2 - \varepsilon_1}(\sigma_{02} - \sigma_{20})$, we have

$$\begin{aligned} S_2 &= -i\int_{-\infty}^{0} \mathrm{d}t \frac{\sqrt{2}\Omega^2}{\varepsilon_2 - \varepsilon_1}(\sigma_{02}\, \mathrm{e}^{-\mathrm{i}\varepsilon_2 t} + \sigma_{20}\, \mathrm{e}^{\mathrm{i}\varepsilon_2 t}) \\ &= \frac{\sqrt{2}\Omega^2}{(\varepsilon_2 - \varepsilon_1)\varepsilon_2}(\sigma_{02} - \sigma_{20}). \end{aligned} \tag{B.5}$$

Thus, $H' = H_0 + H_1 + [V, S_1]/2$ is given by

$$H' = \left(\varepsilon_1 - \frac{2\Omega^2}{\varepsilon_2 - \varepsilon_1}\right)\sigma_{11} + \left(\varepsilon_2 + \frac{2\Omega^2}{\varepsilon_2 - \varepsilon_1}\right)\sigma_{22} + \Omega(\sigma_{01} + \sigma_{10}). \tag{B.6}$$

Neglecting $\Omega(\sigma_{01} + \sigma_{10})$, the eigenstates of H' are $|0\rangle$, $|1\rangle$ and $|2\rangle$. Thus, we have

$$\begin{aligned} H'|0\rangle &= 0, \\ H'|1\rangle &= E_+|1\rangle, \\ H'|2\rangle &= E_-|2\rangle, \end{aligned} \tag{B.7}$$

where $E_+ = \varepsilon_1 - 2\Omega^2/(\varepsilon_2 - \varepsilon_1)$ and $E_- = \varepsilon_1 - 2\Omega^2/(\varepsilon_2 - \varepsilon_1)$. The resonance condition $E_+ = 0$ leads to the same form of the resonance frequency as equation (38).

Because equation (B.7) is rewritten as

$$\begin{aligned} He^{S_1+S_2}|0\rangle &= 0, \\ He^{S_1+S_2}|1\rangle &= E_+e^{S_1+S_2}|1\rangle, \\ He^{S_1+S_2}|2\rangle &= E_-e^{S_1+S_2}|2\rangle, \end{aligned} \tag{B.8}$$

the eigenstates of H are

$$\begin{aligned} e^{S_1+S_2}|0\rangle &= |0\rangle, \\ e^{S_1+S_2}|1\rangle &= |+\rangle, \\ e^{S_1+S_2}|2\rangle &= |-\rangle. \end{aligned} \tag{B.9}$$

Up to $O(\Omega)$, $|+\rangle$ is expanded as

$$|+\rangle = (1 + S_1)|1\rangle = |1\rangle - \frac{\sqrt{2}\Omega}{\varepsilon_2 - \varepsilon_1}|2\rangle + \cdots. \tag{B.10}$$

This means that the population of $|2\rangle$ in $|+\rangle$ is $(\frac{\sqrt{2}\Omega}{\varepsilon_2 - \varepsilon_1})^2$, and the decrease of maximum population of the first excited state in Rabi oscillations is $(\frac{\sqrt{2}\Omega}{\varepsilon_2 - \varepsilon_1})^2$. This result is compatible with the one in section 3.

Appendix C. Equation of motion

We use equation (11) with $O = S_{m'n'mn}$ in equation (26) to obtain the equation of motion for $\rho_{m,n,m',n'}$ as

$$\begin{aligned} \dot{\rho}_{m,n,m',n'} = {} & [-i(\omega_{mn} - \omega_{m'n'}) - \xi_{11}m - \xi_{22}n - \xi_{11}^*m' - \xi_{22}^*n']\rho_{m,n,m',n'} \\ & + i\langle N_1\rangle\sqrt{m'+1}\rho_{m,n,m'+1,n'} + i\langle N_2\rangle\sqrt{n'+1}\rho_{m,n,m',n'+1} \\ & - i\langle N_1\rangle\sqrt{m}\rho_{m-1,n,m',n'} - i\langle N_2\rangle\sqrt{n}\rho_{m,n-1,m',n'} \\ & + i\langle N_1^\dagger\rangle\sqrt{m'}\rho_{m,n,m'-1,n'} + i\langle N_2^\dagger\rangle\sqrt{n'}\rho_{m,n,m',n'-1} \end{aligned}$$

$$
\begin{aligned}
&- i\langle N_1^\dagger\rangle\sqrt{m+1}\rho_{m+1,n,m',n'} - i\langle N_2^\dagger\rangle\sqrt{n+1}\rho_{m,n+1,m',n'} \\
&+ \xi_{11}\sqrt{m+1}\sqrt{m'+1}\rho_{m+1,n,m'+1,n'} + \xi_{12}\sqrt{n+1}\sqrt{m'+1}\rho_{m,n+1,m'+1,n'} \\
&+ \xi_{21}\sqrt{m+1}\sqrt{n'+1}\rho_{m+1,n,m',n'+1} + \xi_{22}\sqrt{n+1}\sqrt{n'+1}\rho_{m,n+1,m',n'+1} \\
&- \xi_{12}\sqrt{m}\sqrt{n+1}\rho_{m-1,n+1,m',n'} - \xi_{21}\sqrt{m+1}\sqrt{n}\rho_{m+1,n-1,m',n'} \\
&- \xi_{12}^*\sqrt{m'}\sqrt{n'+1}\rho_{m,n,m'-1,n'+1} - \xi_{21}^*\sqrt{m'+1}\sqrt{n'}\rho_{m,n,m'+1,n'-1} \\
&+ \xi_{11}^*\sqrt{m+1}\sqrt{m'+1}\rho_{m+1,n,m'+1,n'} + \xi_{12}^*\sqrt{m+1}\sqrt{n'+1}\rho_{m+1,n,m',n'+1} \\
&+ \xi_{21}^*\sqrt{n+1}\sqrt{m'+1}\rho_{m,n+1,m'+1,n'} + \xi_{22}^*\sqrt{n+1}\sqrt{n'+1}\rho_{m,n+1,m',n'+1},
\end{aligned}
\tag{C.1}
$$

where $\omega_{mn} = \omega_1 m + \frac{\alpha_1}{2}m(m-1) + \omega_2 n + \frac{\alpha_2}{2}n(n-1)$, and $\langle N_m\rangle$ and $\rho_{m,n,m',n'}$ abbreviate $\langle\phi(0)|N_m(t)|\phi(0)\rangle$ and $\rho_{m,n,m',n'}(t)$, respectively. In the derivation of equation (C.1), we used the fact that N_m in equation (11) can be replaced by [26]

$$
\begin{aligned}
\langle N_1(t)\rangle &= \sqrt{2\gamma_1}\,\cos(\omega_1 l_1)E_{\rm in}(t), \\
\langle N_2(t)\rangle &= \sqrt{2\gamma_2}\,\cos(\omega_2 l_2)E_{\rm in}(t).
\end{aligned}
\tag{C.2}
$$

The replacement is valid because the initial coherent state is an eigenstate of the noise operator in equation (10).

For the simulations in section 4, we numerically solved equation (C.1) moving to a rotating frame at $\omega_{\rm d}$ for the DQ and the JQF with the use of the rotating wave approximation. We used a fourth-order Runge–Kutta integrator with the time step of less than 0.18 ps. We confirmed the convergence of the numerical results by checking the convergence of the time dependence of p_1 as the time step is decreased. For example in figure 2, the maximum value of p_1 changes less than 0.001% when we halve the time step.

ORCID iDs

Shumpei Masuda https://orcid.org/0000-0002-8286-1925
Kazuki Koshino https://orcid.org/0000-0002-9754-4463

References

[1] Turchette Q A, Thompson R J and Kimble H J 1995 *Appl. Phys.* B **60** S1
[2] Nakamura Y, Pashkin Y A and Tsai J S 1999 *Nature* **398** 786
[3] Blais A, Huang R-S, Wallraff A, Girvin S M and Schoelkopf R J 2004 *Phys. Rev.* A **69** 062320
[4] Wallraff A, Schuster D I, Blais A, Frunzio L, Huang R S, Majer J, Kumar S, Girvin S M and Schoelkopf R J 2004 *Nature* **431** 162
[5] Astafiev O, Inomata K, Niskanen A O, Yamamoto T, Pashkin Y A, Nakamura Y and Tsai J S 2007 *Nature* **449** 588
[6] Majer J *et al* 2007 *Nature* **449** 443
[7] Sillanpää M A, Park J I and Simmonds R W 2007 *Nature* **449** 438
[8] Astafiev O, Zagoskin A M, Abdumalikov A A Jr, Pashkin Y A, Yamamoto T, Inomata K, Nakamura Y and Tsai J S 2010 *Science* **327** 840
[9] Devoret M H and Schoelkopf R J J 2013 *Science* **339** 1169
[10] Kelly J *et al* 2015 *Nature* **519** 66
[11] Ofek N *et al* 2016 *Nature* **536** 441
[12] Shen J-T and Fan S 2005 *Phys. Rev. Lett.* **95** 213001
[13] Hoi I-C, Wilson C M, Johansson G, Palomaki T, Peropadre B and Delsing P 2011 *Phys. Rev. Lett.* **107** 07360
[14] van Loo A F, Fedorov A, Lalumiére K, Sanders B C, Blais A and Wallraff A 2013 *Science* **342** 1494
[15] Forn-Díaz P, García-Ripoll J J, Peropadre B, Orgiazzi J-L, Yurtalan M A, Belyansky R, Wilson C M and Lupascu A 2017 *Nat. Phys.* **13** 39
[16] Zheng H, Gauthier D J and Baranger H U 2013 *Phys. Rev. Lett.* **111** 090502
[17] Paulisch V, Kimble H J and González-Tudela A 2016 *New J. Phys.* **18** 043041
[18] Fang Y-L and Baranger H U 2015 *Phys. Rev.* A **91** 053845
[19] Houck A A *et al* 2008 *Phys. Rev. Lett.* **101** 080502
[20] Koshino K and Nakamura Y 2012 *New J. Phys.* **14** 043005
[21] Hoi I-C, Kockum A F, Tornberg L, Pourkabirian A, Johansson G, Delsing P and Wilson C M 2015 *Nat. Phys.* **11** 1045
[22] Chang D E, Jiang L, Gorshkov A V and Kimble H J 2012 *New J. Phys.* **14** 063003
[23] Lalumiére K, Sanders B C, van Loo A F, Fedorov A, Wallraff A and Blais A 2013 *Phys. Rev.* A **88** 043806
[24] Mirhosseini M, Kim E, Zhang X, Sipahigil A, Dieterle P B, Keller A J, Asenjo-Garcia A, Chang D E and Painter O 2019 *Nature* **569** 7758
[25] Mirhosseini M, Kim E, Ferreira V S, Kalaee M, Sipahigil A, Keller A J and Painter O 2018 *Nat. Commun.* **9** 3706
[26] Koshino K, Kono S and Nakamura Y 2020 *Phys. Rev. Appl.* **13** 014051
[27] Kono S, Koshino K, Lachance-Quirion D, van Loo A F, Tabuchi Y, Noguchi A and Nakamura Y 2020 *Nat. Commun.* **11** 3683
[28] Koch J *et al* 2007 *Phys. Rev.* A **76** 042319
[29] Gea-Banacloche J 2013 *Phys. Rev.* A **87** 023832